Nonlinear Phenomena in Complex Systems, vol. **26**, no. 4 (2023), pp. 393 - 400

Optimization of Electrical Conductivity of the Anodic DLC Coating of Charged Particle Detector

I. A. Zur,[1,*] A. S. Fedotov,[2] A. A. Kharchanka,[1] Y. E. Shmanay,[1] J. A. Fedotova,[1] and S. A. Movchan[3]

[1]*Institute for Nuclear Problems of Belarusian State University, Minsk, BELARUS*
[2]*Department of Computer Modeling, Belarusian State University, Minsk, BELARUS*
[3]*Laboratory of High Energy Physics, Joint Institute for Nuclear Research, Dubna, RUSSIA*

We consider a mathematical model that predicts the electric conductivity of anodic resistive coatings in a charged particle detector and ensures the removal of electron charge in a time shorter than the electron avalanche period. The model is based on the equations for non-stationary electrical current in solids and implemented in COMSOL Multiphysics finite-element code. The model allowed us to establish a correlation between the duration of the avalanche time τ, the amplitude of the current pulse j_{max}, and the electrical conductivity σ. The model predicted that for a thick gas elecrton multiplier detector with a standard gain about 10^4 order and a thickness of coating 100 nm, the conductivity σ should be in the range $(2...5)\cdot 10^{-7}$ S/m in order to ensure that current does not exceed the breakdown value that lies in the range $\sim$1.5 μA. This allowed us to define the most appropriate regime of charged particle detector functioning that combines a high rate of operation and resistance to coating erosion in a detector. The obtained results will be useful for the improvement of the time resolution of charged particles detection in well-type detectors.

PACS numbers: 02.30.Hq, 02.70.-c
Keywords: nanoscale resistive coatings, DLC, charged particle detectors, numerical optimization algorithms, specific electrical conductivity of coatings
DOI: https://doi.org/10.5281/zenodo.10410196

1. Introduction

Breakdown discharges in Gas Electron Multipliers (GEM) lead to deterioration of its sensitivity and performance, degradation of the amplifying element, and, subsequently, the failure of a detector [1–3]. One of the methods of increasing the resistance of gas-discharge detectors to breakdown is the application of resistive coatings on the electrodes, which prevent the development of the arc stage of breakdown due to the local decrease of the voltage in the gas gain region [4–6]. A lot of studies are devoted to the investigation of Diamond-like carbon (DLC) as a resistive coating, so we consider material parameters for DLC in this study. Experimental tuning of GEM detector sensitivity and stability by deposition of a resistive anodic coating is a time-consuming and energy-intensive process. In this regard, it is important to establish the correlation between the electronic characteristics of resistive coatings and the time of electric charge removal by using a mathematical model, which will improve the stability of GEM operation and increase its service life.

The goal of the study is to determine the range of the resistive coating's conductivity σ which would ensure the removal of an electron charge in a time less than the period between subsequent electron avalanches. The use of coatings with conductivity in the mentioned range will guarantee non-overlapping between signals from two subsequent avalanches and improve the time resolution of the GEM detector. On the other side, too fast charge removal may lead to higher current densities exceeding the breakdown discharge values, which leads to erosion of the resistive coating and the failure of a detector.

The proposed mathematical model

*E-mail: E-mail:zur.ilya01@gmail.com

establishes a correlation between the physical characteristics of the coating, in particular, electric conductivity σ and permittivity ε, and the operation parameters such as the time τ of the electron current transfer through the resistive coating and its amplitude j_{max}.

2. Problem statement

In accordance with the standard scheme, shown in Figure 1, the thick GEM detector (THGEM) [4, 7] consists of a gas volume where the X-ray photons $h\nu$ of the ^{55}Fe source cause primary ionization of the working gas atoms (Ar), generating electrons e. The primary ionization electron cloud will drift under the influence of the electric field created by the potential difference U_1-U_2, after which an avalanche-like multiplication of electrons occurs in the holes (wells) of the GEM amplifier board (under the influence of the potential difference U_2-U_3). After the avalanche-like multiplication, the electron cloud drifts from the gas volume to the electrode with a resistive coating under the influence of the potential difference U_3-U_4. There are many factors that influence the spatial resolution of GEM, including convective flow in gas mixture [8, 9], while the time resolution is governed by the electrical properties of anodic electrode coating.

The amplitude of the current I ($\sim 1{\cdot}10^{-7 \div -6}$ A), flowing through the detector at the spark stage of the gas discharge, is known from the experiment [1]. This value was taken as the upper bound I_{max} in calculations of allowed currents. For the lower limit of the current, we have taken the value I_{min} $\sim 1{\cdot}10^{-7}$ A, where the mean period between successive electrical avalanches $T_{av} = 0.25{\cdot}10^{-3}$ s was estimated from the equation [10]:

$$I_{min} = \frac{q}{T_{av}}, \tag{2.1}$$

where q is the charge in an avalanche.

The physical limitation of the I_{min} value originates from the fact that for a too low current, it would be impossible for the charge to be removed before the next avalanche comes. Therefore, I_{min} value indirectly determines the time resolution of the detector under the operational conditions.

One can approximate the cross-section of the current channel with a circle of a diameter equal to the diameter D_{hole} of the hole in the amplifying element (100 μm in our case), so that the allowed values of the current density are in the range $10^0 < j < 10^2$ A/m^2.

3. Mathematical model of electron charge removal through a resistive coating

The mathematical model of charge transfer is based on a system of differential equations (3.1) for charge conservation [11]:

$$\begin{cases} \boldsymbol{j} = \sigma \boldsymbol{E} + \frac{\partial \boldsymbol{D}}{\partial t} + \boldsymbol{j}_{ext}, \\ \boldsymbol{E} = -\bigtriangledown \varphi, \\ \boldsymbol{D} = \varepsilon_0 \varepsilon \boldsymbol{E}, \\ \bigtriangledown \cdot \boldsymbol{j} = -\frac{\partial q}{\partial t}, \end{cases} \tag{3.1}$$

where $\boldsymbol{D}$ is the electric displacement field; j_{ext}

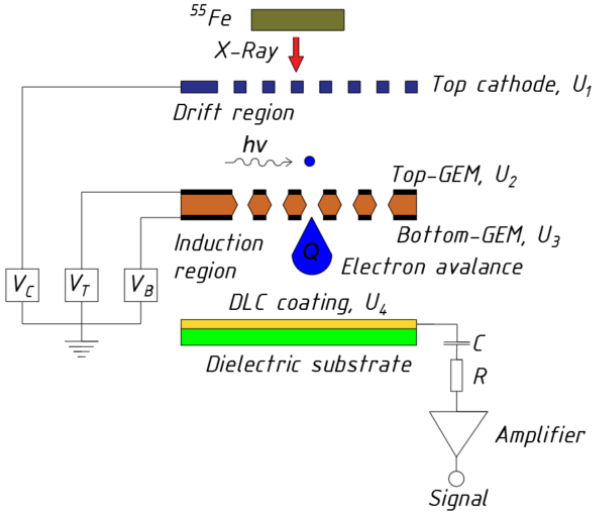

FIG. 1. (Color online) Schematic diagram of an experimental setup for testing GEM detectors.

is the injection current; $\boldsymbol{E}$ is the electric field; ϕ is the electrical potential; q is the electric charge density; $\varepsilon_0 = 8.85{\cdot}10^{-12}$ is vacuum permittivity, ε – dielectric permeability of the resistive coating known for DLC $\varepsilon = 2.2$ from ellipsometry measurements.

The maximum allowed charge Q_{max} that can be removed through the resistive coating is determined by the current density j. Therefore, in order to achieve the fastest charge removal from the gas region (characteristic time τ), it is necessary to increase the density of the injected current j_{ext} while conserving Q_{max}. This current pulse j_{ext} initialized at the boundary DLC-Ar is approximated by Gaussian functions for the spatial $gp(x)$ and temporal $an(t,\tau)$ current distribution. As can be seen from the system of equations (3.2), τ value depends on the coating electrical conductivity σ and dielectric permeability ε:

$$\begin{cases} \boldsymbol{j}_{ext} = \dfrac{Q_{max}}{t} an(t,\tau) gp(x), \\ Q_{max} = e n_0 k_g, \\ an(t,\tau) = \dfrac{1}{\sqrt{2}\tau} \exp\left(\dfrac{t-\tau}{\sqrt{2}\tau}\right)^2, \\ gp(x) = \exp\left(\dfrac{-(x-x_0)^2}{2\sigma^2}\right), \\ \tau = \dfrac{\varepsilon_0 \varepsilon}{\sigma}, \end{cases} \tag{3.2}$$

where Q_{max} is the initial amount of an electrical charge that is concentrated at the interface DLC-Ar, e is the elementary charge, n_0 is mean number of primarily ionized electrons (≈230 electron/photon) that are generated by a single X-ray photon with energy $E_{h\nu} = 5.9$ keV, k_g is the standard gas gain coefficient $1{\cdot}10^4$, $gp(x)$ is Gaussian function normalized by unit area.

When the electron avalanche cloud, shown in Figure 1, reaches the resistive coating, the process of electron injection into the coating volume begins. According to the results obtained in the works of M. Dixit [7, 10], the rate of the charge flow through the coating is determined by the electrical resistivity and the coating capacity. The process of charge propagation in a resistive coating is described by the fundamental solution of the diffusion equation [12] with respect to the charge density. The charge spatial distribution at the boundary governed by $gp(x)$ contribution to a j_{ext} (Eq. (3.2)) is given in Figure 2.

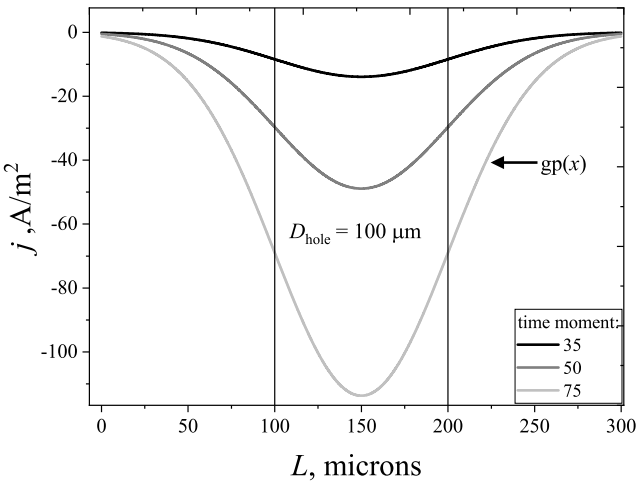

FIG. 2. (Color online) Spatial distribution of the electron current $gp(x)$ across the boundary of the resistive coating at different time moments.

In order to find the optimal characteristic time τ with the finest time resolution, we have to define the objective function (OF). OF serves as a criteria for the maximization process and allows the comparison between different configurations of a system under the optimization process. We chose the peak amplitude of the injection current as the OF, which is calculated as the integral Q_{int} of the normal component of the injection current density j_{ext} across the boundary between the DLC and the metallic layer. The conductivity σ of the DLC plays the role of an independent parameter that governs the Q_{int}. The relations between the OF and current through the internal boundary DLC-metal are given in Eq. (3.3).

For the system (3.1) the following boundary conditions were set. The potential at the upper electrode was fixed as $U_{top} = 100$ V (lower metallization of the amplifying element). The boundary condition on the metal layer is given by the expression (3.3), where the reference voltage U_{ref} is equal to the initially applied voltage U_{met}

= 1000 V.

$$\begin{cases} Q_{int} = \int\limits_0^L \boldsymbol{j}(\sigma) dl, \\ n \cdot \boldsymbol{j}(\sigma) = \left(\sigma_{met} + \varepsilon_0 \varepsilon \dfrac{\partial}{\partial t}\right) \dfrac{U - U_{ref}}{d_{met}}, \\ U_{ref} = U_{met}, \end{cases} \tag{3.3}$$

where σ is the electrical conductivity (or reciprocal resistivity ρ^{-1}), dl and L – elementary linear section and the integration limit, σ_{met} and d_{met} – the electrical conductivity and the thickness of the metal layer.

4. Numerical solution methods

Partial differential equations for the transient problem of electron transport were time-integrated using the backward differentiation formula (BDF) method – the implicit five-step method [13]. Spatial discretization of Eqs.(3.1) was performed with the finite-element method with linear basis functions. The resulting systems of linear algebraic equations were solved by a MUMPS solver [14]. The variational problem of finding the extreme value of the integral objective function was solved using the Monte Carlo algorithm with a uniformly distributed probability of parameter selection. The duration of the time-integration process was performed until time 8τ, which ensured that the whole excessive charge is removed.

An equivalent electrical circuit for the detector part consisting of a gas gap and an electrode with a resistive DLC coating is a resistor and capacitor connected in parallel. The discharging process inside can be described as an exponential function of time.

Figure 3 shows the exponential and Gaussian functions for the equivalent electrical circuit discharging process. It is seen that at the moment when the exponential function reaches the relaxation time, the value of the function is equal to 0.38 of the maxima, while the area under the curve in Figure 3a is 62% of the total integral of the function, the Gaussian function in Figure 3, b, by 1 "sigma" is 68% of the total value of the integral, and the function has a value of 0.6 of the maximum value. It can be seen that the approximation in the form of a Gaussian function for the current sweeping time does not introduce a significant error in the description of the process.

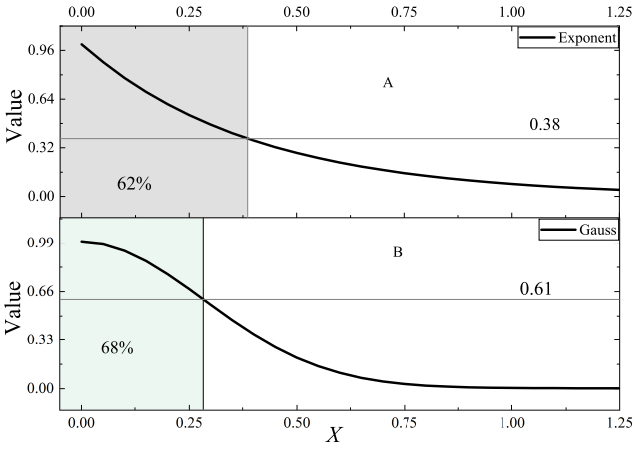

FIG. 3. (Color online) Comparison exponential (a) and Gaussian (b) functions for equivalent electrical circuit discharging process.

The computational domain is shown in Figure 4. It consists of three regions: the resistive DLC coating with a thickness $d = 100$ nm, the dielectric substrate with a thickness of 10 μm and the Ar gas gap with a thickness of 200 μm. The metallic electrode is set as a boundary condition to simulate contact with the outer copper layer. The computational domain was discretized by the Delaunay triangulation method [15], which resulted to $340{\cdot}10^3$ finite elements. To increase the accuracy of the calculation, additional $32{\cdot}10^3$ elements were inserted into the DLC coating area. The average quality of the elements is 0.87 by the isogonality criterion of the triangular elements (with a maximum of 1) [15]. Figures 4 and 5 show the computational domain boundary conditions and the calculated mesh near the boundary of the resistive coating.

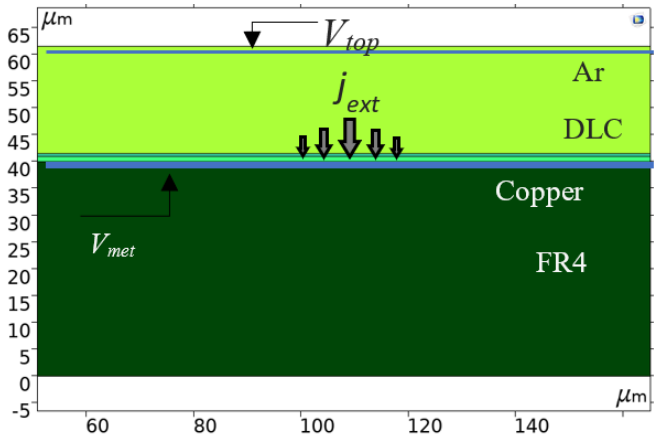

FIG. 4. (Color online) Geometric regions of the computational domain: Ar – gas gap, DLC – resistive layer, copper – copper electrode (not in scale), $FR4$ – dielectric substrate. Boundary conditions: for the potential of the upper and metal electrodes V_{top} and V_{met} correspondingly, and for the injected current density j_{ext}.

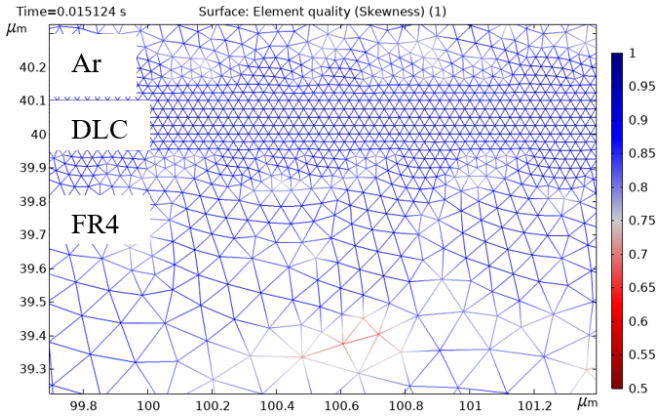

FIG. 5. (Color online) Image of the calculated mesh near the domain of the resistive coating.

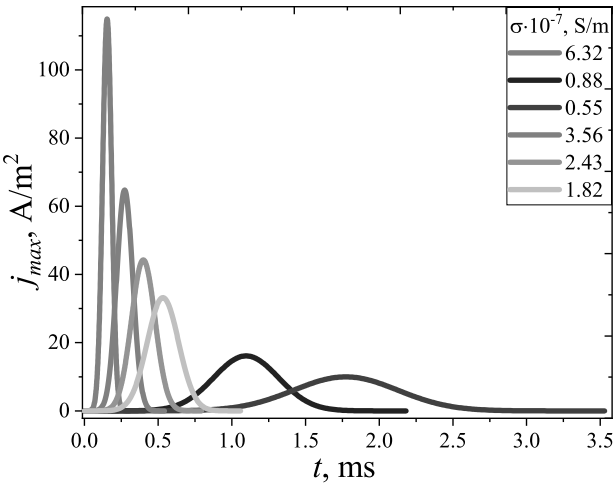

FIG. 6. (Color online) Time dependence of the current density normal component j at the DLC/metallic layer interface for the DLC conductivity σ in range $(5.9 \cdot 10^{-9} - 2.7 \cdot 10^{-6})$ S/m.

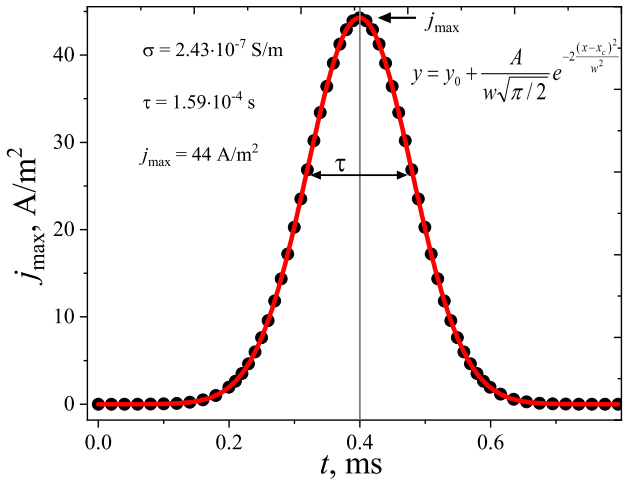

FIG. 7. (Color online) Time dependence of the current density normal component j at the DLC/metal interface for $\sigma = 2.4 \cdot 10^{-7}$ S/m.

5. Results and discussion

As can be seen from Figures 6 and 7, the current pulse duration width τ and the amplitude $j_{max}(\tau)$ are dependent on the value of the DLC conductivity (control parameter) σ.

As was found from numerical experiment, the characteristic time τ monotonically decreases with an increase in the electrical conductivity of the coating σ according to a law close to hyperbolic, Figure 8. At the same time, current density j_{max} increases linearly with σ as is seen in Figure 9.

In the end of paragraph II we estimated that the allowed current density values j_{max} are in range $(10^1 - 10^2)$ A/m^2. The allowed range of current density is highlighted in cyan in Figure 10. From one side, it can be seen that the DLC

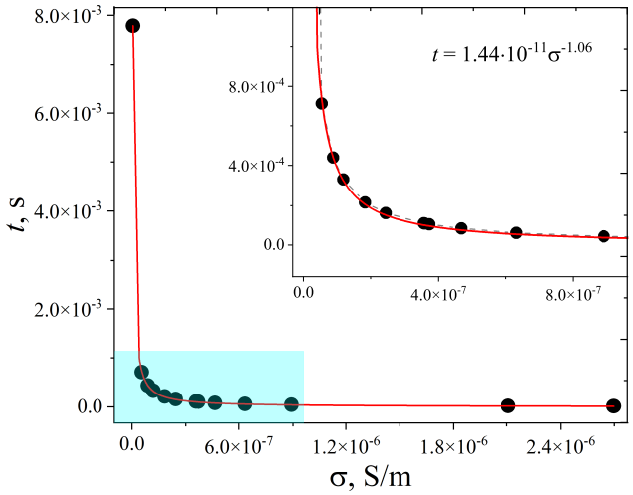

FIG. 8. (Color online) Dependence of the pulse characteristic time τ on DLC conductivity σ.

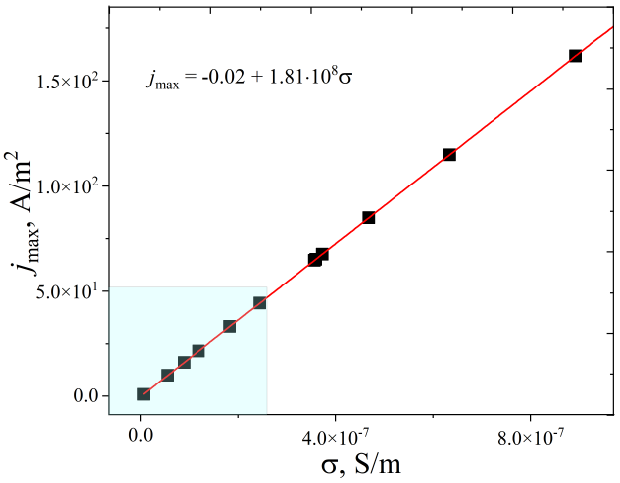

FIG. 9. (Color online) Dependence of the current density amplitude j_{max} on the DLC conductivity σ. Blue box: area, in which current pulse does not cause the breakdown

coatings with a value of $\sigma \lesssim 2 \cdot 10^{-7}$ S/m have a time of charge removal longer than the period between avalanches, which leads to a critical decrease in the time resolution of the detector. When the σ value is higher than $6{\cdot}10^{-7}$ S/m, the current density exceeds a critical value, which leads to the spark breakdown stage and DLC coating erosion.

When the injected current density j starts

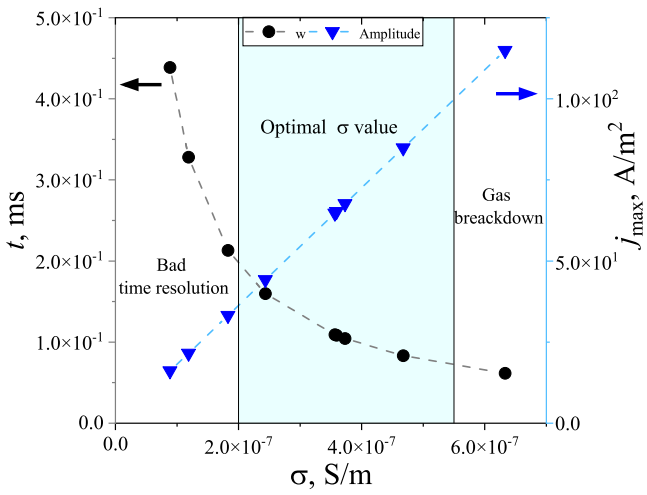

FIG. 10. (Color online) Dependence of characteristic time τ and current density j_{max} on the electrical conductivity σ DLC-coatings for the range $(1 \leq \sigma \leq 6) \cdot 10^{-7}$ S/m.

flowing through the resistive coating, a local voltage drop is created on the DLC (see Figure 11), which distorts the initial (at $t = 0$) external potential difference U_3-U_4 between the electrodes. It can be seen that the magnitude of this potential distortion can reach values of $\sim 10^1$ V. Figure 12 demonstrates the example of both the pulse shape distortion and delay in time between the current and the voltage for the mean value of injected current j in the domain around the resistive coating, which we explain by the capacitive properties of the DLC coating.

When current flows through the resistive DLC coating, it causes the Joule heating. To consider the thermal effects, we should add the integral equation for heat balance [12]:

$$\Delta\Theta \approx \frac{1}{\sigma c m} \int_0^T \left(\int_0^S j(x,t) dS \right)^2 dt, \quad (5.1)$$

to the system of differential equations (3.1). Here $\Delta\Theta$ is the overheating due to c and m are heat capacity and mass of the DLC coating, L and T – limits of integration with respect to spatial and temporal variables: the length of the region and the pulse duration, respectively. As follows from

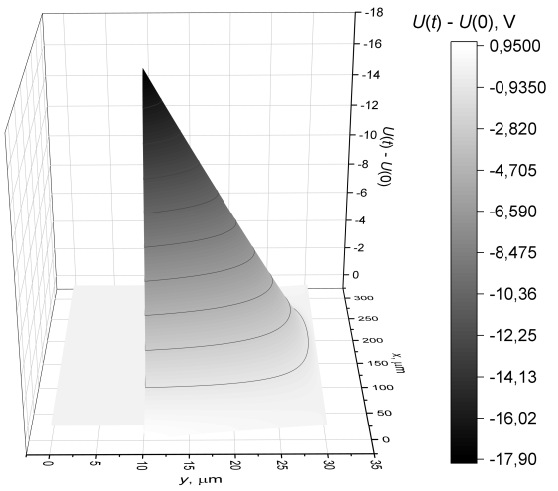

FIG. 11. (Color online) The potential distortion within of maximum current density.

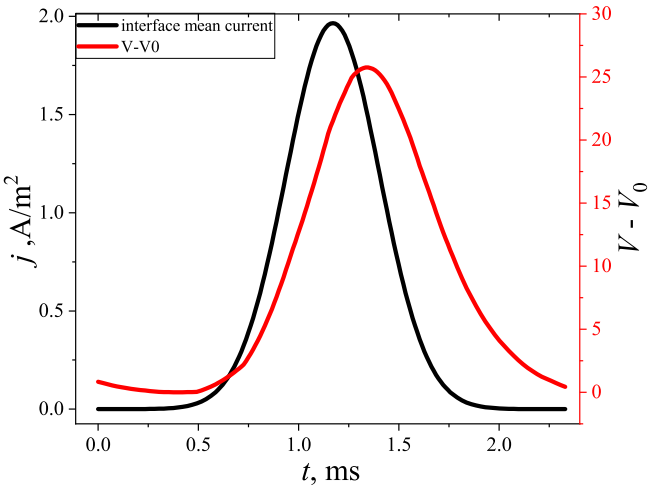

FIG. 12. (Color online) Time dependence of the mean value of the injected current and voltage drop in the domain of around the resistive coating.

(5.1), the overheating per one avalanche can reach values $\Delta\,\Theta \sim 10^{-2}$ K.

In future works, the process of ohmic heating of the DLC coating will be taken into account, which will affect the specific electrical conductivity σ, therefore the transport of electrons in the coating and the magnitude of the local voltage drop.

6. Conclusion

We developed the mathematical model, which established the correlation between the time of electric charge removal and the peak magnitude of injected current in a nanoscale resistive DLC coating of the collector electrode in the GEM detector and its electrical conductivity. This model was based on a system of differential equations that was solved by the finite element method.

We estimated the conductivity of anode coating σ suitable for the optimal regime of functioning of the detector. Coatings with σ in the range of $(2 - 5.5) \cdot 10^{-7}$ S/m allow the electron charge to be removed in less time than the avalanche period when the current density j is below the critical value ($\sim 10^2$ A/m^2). The higher conductivity leads to higher current densities, which cause the erosion of the DLC coating and the failure of the detector. The lower DLC conductivity makes the removal of charge too slow, so the temporal resolution of the detector decreases until it fails to distinguish separate breakdown events due to electron detection.

We also studied the spatial distribution of the potential near the electrodes of the detector and its dependence on the amplitude current density j_{max} during the breakdown. It was found that the capacity of the DLC coating governs the observed time delay between the peaks of current and voltage during the breakdown.

The results obtained will be useful in improving the time resolution of charged particle detectors. The authors acknowledge the financial support of Joint Institute for Nuclear Research (JINR) under contracts N08626319/201142470-74 (2021) and N08626319/2011293539-74 (2022). The authors also acknowledge the contribution of the Student Research Laboratory "Computational experiment and gametech"of Belarusian State University to this research.

References

[1] A. Jash, L. Moleri, and S. Bressler. arXiv preprint arXiv:2204.09445 (2022).

[2] B. Ulukutlu, P. Gasik, T. Waldmann, L. Fabbietti, T. Klemenz, L. Lautner, R. de Oliveira, and S. Williams. Nuclear Instruments and Methods in Physics Research Section A: Accelerators, Spectrometers, Detectors and Associated Equipment **1019**, 165829 (2021).

[3] A. Utrobicic, M. Kovacic, F. Erhardt, M. Jercic, N. Poljak, and M. Planinic. Nuclear Instruments and Methods in Physics Research Section A: Accelerators, Spectrometers, Detectors and Associated Equipment **940**, 262 (2019).

[4] I. Vankov, S. Vasilev, I. Golutvin, Y. V. Ershov, V. Y. Karjavin, A. Makankin, V. Perelygin, and V. Chekhovski. Physics of Particles and Nuclei Letters **10**, 783 (2013).

[5] J. Metcalfe, I. Mejia, J. Murphy, M. Quevedo, L. Smith, J. Alvarado, B. Gnade, and H. Takai. arXiv preprint arXiv:1411.1794 (2014).

[6] V. Peskov, B. Baibussinov, S. Centro, A. Di Mauro, B. Lund-Jensen, P. Martinengo, E. Nappi, R. Oliveira, F. Pietropaolo, P. Picchi, et al.. IEEE Transactions on Nuclear Science **54**, 1784 (2007).

[7] *Nica multi purpose detector*, `https://nica.jinr.ru/ru/projects/mpd.php`, accessed: 2022-10-24.

[8] A. Fedotov, Y. Tsitavets, and A. Elyshev. Case Studies in Thermal Engineering **41**, 102606 (2023), URL `https://doi.org/10.1016/j.csite.2022.102606`.

[9] Y. D. Tsitavets, A. S. Fedotov, S. A. Movchan, I. A. Balashov, A. A. Makarov, and V. V. Chepurnov. Memoirs of the Faculty of Physics (2020).

[10] M. S. Dixit, J. Dubeau, J. P. Martin, and K. Sachs. Nuclear Instruments and Methods in Physics Research Section A: Accelerators, Spectrometers, Detectors and Associated Equipment **518**, 721 (2004).

[11] A. S. Fedotov, V. Shepelevich, S. Poznyak, L. Tsybulskaya, A. Mazanik, I. Svito, S. Gusakova, P. Zukowski, and T. N. Koltunowicz. Materials Chemistry and Physics **177**, 413 (2016), URL `https://doi.org/10.1016/j.matchemphys.2016.04.047`.

[12] A. N. Tikhonov and A. A. Samarskii. *Equations of mathematical physics* (Courier Corporation, 1999).

[13] *Bdf, generalized alpha, and runge-kutta methods*, `https://www.comsol.ru/support/knowledgebase/1062`, accessed: 2022-10-24.

[14] *MUMPS : a parallel sparse direct solver*, `https://graal.ens-lyon.fr/MUMPS/index.php`.

[15] *COMSOL Multiphysics Reference Manual*, COMSOL Software License Agreement (2020).